Tunable rheological-tribological performance of “green” gel-like dispersions based on sepiolite and castor oil for lubricant applications

J.E. Martín-Alfonso*, M.J. Martín-Alfonso, J.M. Franco

Department of Chemical Engineering and Materials Science, Campus de “El Carmen”, University of Huelva, Chemical Product and Process Technology Research Center (Pro^{2}TecS) 21071 Huelva, Spain.

* Corresponding author. Present address: Department of Chemical Engineering and Materials Science, 21071 Huelva, Spain. Tel.: +34 9598204; fax: +34 959219385.

E-mail address: jose.martin@diq.uhu.es (J.E. Martín-Alfonso)

ABSTRACT

This work has been focused on the preparation and characterization of gel-like dispersions based on sepiolite and castor oil potentially suitable as eco-friendly lubricating greases. Particularity, the effect of sepiolite content exerted on rheological, chemical, thermal and tribological properties was studied. The system exhibited a gel-like behaviour for all the concentrations considered (20–40 wt.%) related to the development of a sepiolite three-dimensional colloidal network due to its characteristic nanoscale structure formed by fibers, laths and bundles. The values of both apparent viscosity and viscoelastic functions in the linear viscoelastic region increased with sepiolite content, as a consequence of a strengthening of the gel network. An empirical correlation between “plateau” modulus and sepiolite concentration was proposed. From tribological point of view, the friction coefficient values and wear marks obtained after the frictional tests became lower when sepiolite concentrations decrease. Gel-like dispersion formulated with 30 wt.% sepiolite showed appropriate rheological and tribological behaviour to be used as biolubricating greases.

Keywords: Sepiolite; Vegetable oil; Rheological properties; Tribology; Chemical properties

1. Introduction

Global widespread concern about environmental pollution and climate change has guided modern research toward “green” materials science and technology. Therefore, and more commonly at the present time, there are a great need of producing bio-based and biodegradable materials suitable to be used as lubricants in order to minimize the contamination damage that synthetic or fossil fuel-derived products cause in the environment. Lubricating greases are generally highly structured colloidal dispersions that possess two phase structure consisting of a thickener or gelling agent, generally metal soaps, and a fluid oil lubricant. The thickener forms a colloidal network, which traps the oil into its micro-nano structure and allows the grease to exist in the semi-solid state. The desired gel-like characteristics and, specifically, appropriate thermorheological and tribological properties of lubricating greases depend on the nature of components and the microstructure perfomed during its processing (Martin-Alfonso et al., 2013a). Considering that lubricant greases are the most widely used lubricants in rolling element bearing applications, finding a new formulations with suitable properties may create a new market niche with interesting perspectives in the future. So far, the majority components of lubricating greases are considered non-renewable materials, the challenge in lubricating greases engineering is the development of new to total or partially replace formulations based on renewable materials in order to produce fully biodegradable lubricating greases. One interesting strategy to improve this issue is to make lubricating greases based on vegetable oils and inorganic nanoclays, given that they are considered environmentally friendly materials (Ray and Bousmina, 2005) and have the ability for swelling and gel formation in organic media (Chtourou et al., 2006). There are different types of inorganic nanoclay on basis of their sheet arrangement (Bergaya et al., 2006) such as halloysite, imogolite and sepiolite.

Halloysite and imogolite are nanosized tubular clay and are derived from volcanic origin (Pasbakhsh et al., 2013; Cavallaro et al., 2018; Du et al., 2017). The sepiolite belongs to 2:1 phyllosilicates. The sepiolite has a structural formula $Si_{12}0_{30}Mg_8(OH,F)_4(H_2O)_2.8H_2O$. The sepiolite exhibits fibrous/needle morphology with dimensions ranging from 100 to 5000 nm length, 10–30 nm width and 5–10 nm thickness which are the main reason for the characteristic properties of this clay mineral (Ruiz-Hitzky et al., 2011; Olivato et al., 2015). The sepiolite is made up of two tetrahedral silica sheets sandwiching a central octahedral magnesium oxide-hydroxide sheet. Silanol (Si-OH) groups are present in the longitudinal direction of rectangular channels (Ruiz-Hitzky et al., 2013). The density of silanol groups on sepiolite is 2.2 /100 angstrom square. These silanol groups are located along the side of the external channels after every 0.5 nm. The coordinated water and zeolitic water molecules are present in these channels (Masood et al., 2019). Due to its unique structure and morphology, sepiolite is widely used in a variety of industrial applications (Sabah, 2007), such as catalyst carriers (Güngör, et al., 2006; Núñez, et al., 2014), adsorbents (Rytwo, et al., 2002; Özdemir, et al., 2007), as a rheological additive in water-based drilling fluids (Weng, et al., 2018; Zhuang, et al., 2018), for removal of organic contaminants in water (Rytwo, et al., 2011), or development of polymer/clay nanocomposites (Darder et al., 2017; Fernandez-Barranco, et al., 2016; Mejía, et al., 2014). In addition, another possible application of this nanoclay may result from its capacity to form gel-like dispersions with tunable mechanical properties. Because of the fibrous morphology, sepiolite fibers can disperse well in high-polarity solvents and build colloidal network structure, resulting in excellent rheological and tribological properties. One of the advantages of sepiolite, compared to “conventional” clays based on layered silicates (i.e., smectites and vermiculites) is the high density of surface

silanol groups (Si-OH), which allows hydrogen bonding interactions at the silicate interacting with diverse organic species (Castro-Smirnov et al, 2016). Thus, when the sepiolite is added into the base oil, the Si-OH groups could promote the dispersion and interfacial interaction of sepiolite with the molecular chain of the oil to form an oil-retentive pore network.

Recently, the development of gel-like dispersions to formulate eco-friendly lubricating greases has received significant attention. In particular, cellulose pulp from Eucalyptus has been proposed as a promising green thickener of vegetable oil media (Nuñez et al., 2012a). However, some limitations regarding the physical (under static conditions) or mechanical (after shearing or shaking) stability were still found in physically-stabilized dispersions (Nuñez et al., 2012b), even when reducing polarity by means of methylation (Martín Alfonso, et al., 2009) or ethylation (Martín-Alfonso, et al., 2011) to increase compatibility with the oil medium. Significant improvement in both rheological properties and mechanical stability were obtained by inducing chemical crosslinking between cellulose pulp and castor oil by means of adding diisocyanate compounds (Gallego, et al., 2015). Nevertheless, to the best of our knowledge, no reports exist dealing with the formulation and characterization of gel-like dispersions based on sepiolite and castor oil blends. In this context, the main objective of this study was to evaluate the use of sepiolite as thickener agent to formulate gel-like dispersions for applications as eco-lubricating greases. With this aim, rheological, chemical, and thermal characterizations, as well as tribological evaluation have been carried out, focusing on the influence of thickener concentration on the rheological behavior, in order to evaluate the suitability of these formulation as new eco lubricants.

2. Materials and methods

2.1. Materials

Castor oil (211 cSt at 40ºC, Guinama, Spain) was used as biodegradable lubricating oil for formulations of gel-like dispersions. A commercially available sepiolite without modification ("Sep", hereinafter) purchased by Sigma-Aldrich without any chemical treatment was used as thickener agent in oil media. A model bentonite lubricating grease (Verkol S.A., Spain) was used as benchmark.

2.2. Preparation of gel like dispersions

The processing of dispersions was prepared by mixing, at room temperature, the sepiolite in castor oil, using a rotor-stator turbine (Ultra Turrax T-50, Ika, Staufen, Germany) at 9000 rpm for 10 minutes. Prior to their high shear processing, the sepiolite was wetted with the oil for 60 minutes, at room temperature. Sepiolite concentration in the blend was in the range of 20-40 wt.%.

2.3. Characterization methods

Different rheology tests were carried out at 23±0.1 ºC with a Rheoscope controlled-stress rheometer (TermoHaake, Germany) using a rough plate-and-plate geometry (20 or 35 mm diameter, depending on the sample, 1 mm gap, relative roughness 0.4) to evaluate the rheological behaviour of dispersions: (a) oscillatory stress sweep tests, at a frequency of 1 Hz ($\omega = 2\pi f = 6.28$ rad/s), were carried out to find the linear viscoelasticity range; (b) small-amplitude oscillatory shear (SAOS), inside the linear viscoelasticity regime, was performed in a frequency range between 10^{-2} and 10^{2} rad/s; (c) Steady-state viscous flow curves were run according to a shear rate stepwise procedure in a shear rate range (0.01-100 s^{-1}). Viscosity was calculated in each step after a maximum shear time of 200 s, unless the steady-state response had been previously

achieved within 1% tolerance. In addition, the evolution of viscosity as a function of time was also obtained to study the thixotropic behaviour of samples by measuring viscosity of dispersions at alternating high and low shear rates (0.1 and 10 s^{-1} respectively) and finally, (d) recovery tests were carried out to characterize the effects produced by strain conditions on the viscoelastic properties of the dispersions. A time sweep test at 1 Hz was performed, varying the strain over three steps: during the first step, a strain within the linear viscoelastic region was applied; this was followed by a step at a higher strain of 5%; then the first-step conditions were applied again in the final step. In order to ensure accurate results, at least three replicates were conducted for every sample/test and data was expressed as the mean ± standard deviation.

X-ray diffraction tests were carried out at 23 ºC in a D8 Advance X-ray diffractometer (Bruker-AXS, Germany) with Cu-Kα radiation at a generator voltage of 40 kV, a current of 30 mA and a wavelength of 0.15406 nm. The samples were scanned over an angular range of 2θ (1.5–40°), with a scan rate of 2^{o} min^{-1}.

Fourier transform infrared (FTIR) spectra were obtained by means of JASCO FT/IR-4200 apparatus. The spectra were registered within a wavenumber range of 400–4000 cm^{-1} at 4 cm^{-1} resolution in the transmittance mode. A total of 46 scans per sample in the transmission mode were done.

Thermogravimetric analyses were carried out by using a Q-50 TA Instrument under N_2 purge. Approximately, 8 mg of each sample were placed on a Pt pan, and heated from 30ºC to 600ºC at 10ºC/min.

Penetration indexes and NLGI consistency numbers of dispersions tested were determined according to the ASTM D 1403 standard, using the Seta Universal penetrometer, model 17000-2 (Stanhope-Seta, UK), with one-quarter cone geometry.

The one-quarter scale penetration values were converted into the equivalent full-scale cone penetration values following the ASTM D217 standard.

Tribological tests were performed using a tribological cell coupled with a Physica MCR-501- Rheostress rheometer (Anton Paar, Austria). The tribology cell consists of a 1/2 in. diameter steel ball (1.4401 Grade 100, roughness = 0.10 μm) rotating on three 45º inclined steel plates (1.4301, roughness = 0.21 μm). All tests were performed by applying a normal load of 10 and 30 N and constant rotational speed of 100 rpm during 10 minutes at 25ºC. This test was repeated 5 times to obtain an accurate average friction factor. For each test, a new contact area on the surface of the ball was used, and all specimens were cleaned with ethanol. Resulting wear marks in the plates were examined in an Olympus BX52 (Japan) microscope equipped with an Olympus C5050Z camera and an objective of 4x.

3. Results and Discussion

3.1. Rheological behavior of gel-like dispersions

3.1.1 Linear viscoelastic properties

In order to define the upper limit of the linear viscoelastic range (LVR), oscillatory stress sweep tests were conducted. **Fig. 1** shows the dependence of the normalized storage modulus ($G' = G'/G''_{1\ Pa}$) with stress (τ) for gel-like dispersions as function of sepiolite content. The behaviour illustrated in this figure is typical of many viscoelastic materials such as suspensions, gels, emulsions, and polymers: the normalised storage modulus remains constant in the linear range and decreases above a critical shear stress (τ_c), indicating structural breakdown within the gel network of the sample. All the samples studied exhibit a wide range of linear viscoelastic range and it was greatly

influenced by sepiolite content. As can be observed, higher stress is required to disrupt the structure when sepiolite concentration is increased, whereas the critical strain undergoes a slight decrease (see **Fig.1**), reflecting a stronger colloidal network to shear forces. Similar observation has been reported in the case of other gel-like dispersions based on EVA copolymer and vegetable oils (Martín-Alfonso and Franco, 2014; Martín-Alfonso and Valencia, 2015).

Fig. 2 shows the mechanical spectra obtained from frequency sweep tests for dispersions at different sepiolite concentrations. Samples generally showed a gel-like behaviour, where G' is much higher than G'', within the whole experimental frequency range, and the slopes of both viscoelasticity functions vs. frequency showed a moderate dependence. This behaviour was very similar to that found with model bentonite lubricating grease and to that shown by other gel-like dispersions previously studied (Nuñez et al., 2012a; Martín-Alfonso et al., 2013a). This mechanical spectrum is typically of systems with physical network structures, in both cases (sepiolite and bentonite), attributed to the colloidal network formed by nanoclays (Maqueda et al., 2009; Galindo-Rosales and Rubio-Hernández, 2006). However, at lowest sepiolite content, higher slopes with frequency were found, as well as a tendency to undergo a crossover point between both moduli at high frequency, which reveals a weakening of the elastic network. On the other hand, as can be observed in **Fig. 2b**, the loss tangent ($\tan \delta = G''/G'$) values depend on sepiolite content in the whole frequency range studied, indicating that the relative elastic characteristics of these gel-like dispersions increase by increasing sepiolite concentration.

Fig. 3 summarizes the effect of sepiolite content on the linear viscoelastic response of gel-like dispersions through the evolution of parameters G'_1, G''_1 and $\tan \delta_1$ obtained

from the mechanical spectrum at 1 rad/s, as a function of sepiolite concentration. As can be observed, storage and loss viscoelastic moduli clearly increase with sepiolite concentration and its evolution can be fitted to a power-law equation:

$$G_1 = a \cdot (wt.\%Sep)^b \quad (1)$$

where a and b are fitting parameters. Tan δ values linearly decrease with sepiolite concentration This behaviour could be explained in terms of the physical interactions between the components of the dispersions, sepiolite particle density increases with sepiolite concentration and in the same sense increases the degree of interactions among entangled fibers, laths and bundles.

3.1.2 Viscous flow behavior and thixotropic properties

Fig. 4a shows the flow curves of gel-like dispersions at different sepiolite concentration. These flow curves were obtained from a single sweep using the controlled strain mode of operation of the rheometer. Two problems could be encountered during the measurement of the flow properties of lubricating grease; one is slip at the wall and the other is sample fracture (Yeong et al., 2004). On one hand, slip at the wall or depletion effects occur in the flow of two-phase (or multiphase) suspensions in viscometers (or rheometers) as a result of the displacement of the dispersed phase(s) away from the boundaries (Barnes, 1995). As a result, the rheological value obtained does not necessarily represent the bulk material and is only representative of the depleted layer immediately adjacent to the wall (Magnin, and Piau, 1990). In lubricating grease, wall slip is often detected in the regions where the shear rates are lower than 0.5 or 1 s^{-1} (Magnin, and Piau, 1990). In this case, serrated plate–plate geometry was used in order to eliminate the wall-slip effects usually observed

during the flow of these materials (Martín Alfonso et al., 2013a). On the other hand, sample fracture usually occurs in samples of a higher concentration. This occurs when either the sample has departed from the boundary of the geometry or when cracks form on the edges of the geometry, thus forming some empty spaces in between the gap. This often affects values in the high-shear region and temperature, whereby the measured shear stress or viscosity at the high-shear region is lower than the expected value (Martín Alfonso et al., 2013b). As can be observed, the flow behavior of all gel-like dispersions is characteristic of the viscoelastic materials, showing a shear-thinning response in the low shear rate region with a tendency to reach a limiting viscosity in the high shear rate region. In this case, sample fracture was detected in the samples with 35 and 40 wt.% sepiolite concentrations. The flow behavior follows the Sisko's model fairly well with R^2 values above 0.99:

$$\eta = m\dot{\gamma}^{n-1} + \eta_\infty \quad (2)$$

where "*m*" is a parameter related to the consistency of the sample, "*n*" is a parameter related to the slope of the shear thinning region, being the so-called flow index and η_∞ is the asymptotic viscosity at high shear rates. The fitting parameters are shown in **Table 1**. Gel-like dispersions exhibited an increase of the consistency index values, *m*, with the increase the sepiolite content, obviously, as a consequence of increasing viscosity. On the other hand, the values of the flow index, *n*, were quite close to zero for all the dispersions studied, which is representative of the typical yielding behavior shown by these materials (Yeong et al., 2004). This behavior is characterized by a decay of several decades in viscosity with a very small increment in shear stress.

In addition, shear thinning properties of dispersions were determined by studying the viscosity changes of the gel-like dispersions at low and high shear rates (0.1 and 10 s^{-1}

respectively) over certain duration of time. As can be observed in the **Fig. 4b**, it was found that there was initially a light progressive decrease in the viscosity of samples at a constant low shear rate when measured over a time period of 20 min. When the shear rate was increased to high shear rate, it was showed that the structure was completely broken down with viscosity values dipping. Nevertheless, the structure showed some reformation when the shear rate was changed back to low. These results confirm that these samples showed thixotropic property with a prominent shear thinning as well as partial recovery of structure. This particular property of these gel-like dispersions is interesting for application where a reversible structure breakdown and recovery is desired such as mechanisms of grease lubrication.

3.1.3 Structural recovery

Fig. 5 shows the evolution of the complex modulus (G*), which unifies both elastic (G') and viscous (G'') contributions of the material, for dispersions containing different sepiolite concentrations when a shear strain outside the linear viscoelastic region is applied and the subsequent recovery when a shear strain inside the linear region is again restored. The complex modulus decreases when a shear strain outside the linear viscoelastic range is applied on the sample and subsequently partial or total recovery in the complex modulus values is observed when a shear strain inside the linear range is again restored. The percentage values of recovery and destruction for the dispersions were calculated as follows:

$$destruction = \frac{G_O^* - G_1^*}{G_O^*} \cdot 100 \quad (3)$$

$$recovery = \left(\frac{G_2^* - G_1^*}{G_O^* - G_1^*} \right) \cdot 100 \quad (4)$$

where G_o^* is the complex modulus for the first shear strain applied (inside the linear viscoelasticity region); G_1^* is the complex modulus for the second shear strain applied (outside the linear viscoelasticity region); and G_2^* is the complex modulus for the third shear strain value (inside the linear viscoelasticity region). **Table 1** shows the percentage values, calculated from **Eq-3** and **4**, for the rheo-destruction and recovery of the dispersions. The percentage of rheo-destruction decreased with the sepiolite content, while the percentage of recovery increased. These results could be explained in terms, on one hand, when the thickener agent network is destroyed, the capacity of this structure to hold a certain amount of base oil is decreased, resulting in separation of the thickener agent and the oil phase and, on the other, as has been previously discussed considering SAOS tests, the values of G' and G'' increase with sepiolite concentration (indicative of a more compact structural network), which appears less sensitive to shear strain applied, reflecting lower values of rheo-destruction and more higher values of recovery. In this context, it has been demonstrated that the level of shear strain plays an important role with respect to the irreversible degradation of the structure of the gel-like dispersions (Lawal, et al., 2011).

3.2 Chemical and thermal properties of gel-like dispersions

Fig. 6 shows FTIR spectra of sepiolite, castor oil and selected gel-like dispersions with different clay contents (20, 30 and 40 wt.%). For the spectrum of castor oil, several characteristic peaks were confirmed, hydroxyl group of the ricinoleate moiety was present at 3380 cm^{-1}, the peaks at 3009 cm^{-1} confirmed the present of C=C. The strong peak occurred at 2926 cm^{-1} and 2852 cm^{-1}, which arose from C-H asymmetric stretch vibration in methylene and methyl group stretching on the chain, the peak at 1745 cm^{-1} was attributed to C=O (carbonyl group) stretching vibration absorption (Liang, et al.,

2019a; Liang, et al., 2019b). For the sepiolite, the main bands in the FTIR spectrum were the following: (i) the adsorption band observed at 3689 cm^{-1} corresponded to the stretching vibration of Mg−OH; (ii) two peaks centered at 3564 cm^{-1} and 3408 cm^{-1} are ascribed to the O−H vibrations of coordinated water and zeolitic water, respectively and (iii) the O-H bending peak at 1663 cm^{-1} is associated with water molecules in channels (Qiu, et al., 2019). Furthermore, the lattice vibrations are given as follows: (i) the adsorption bands at 1212 and 1023 cm^{-1} were ascribed to Si−O vibrations of the Si−O−Si; (ii) the adsorption peak observed at 789 cm^{-1} was due to O-H bending vibration of Mg-Fe-OH (Li et al., 2018); (iii) two peaks centered at 694 and 645 cm^{-1} were attributed to the bending vibration of Mg-OH. These characteristic absorption peaks were also observed in the FTIR spectra of gel-like dispersions. This confirms the presence of all components used to prepare the sample and also indicate the negative formation of new chemical groups between castor oil and sepiolite clay.

In addition, results on X-ray diffraction (XRD) test may shed light on the degree of interaction of sepiolite with castor oil. Thus, X-ray diffraction patterns of the sepiolite and gel-like dispersions with different clay contents are shown in **Fig. 7**. The interlayer d-spacing between clay layers of the samples was obtained by means of the 2θ angle value at which the (001) basal reflection peak is observed, according to the Bragg equation:

$$\sin\theta = \frac{n\lambda}{2d} \tag{6}$$

where λ is the wavelength of the X-ray radiation used in the diffraction experiment, *d* is the interlayer distance, *n* is the order of diffraction, corresponding to an integral multiple of the wavelength, and θ is the angle of incident radiation. As it can be

observed, the main diffraction peak of sepiolite appeared at 2θ=7.31° (110) corresponding to the interlamellar spacing of the clay as d=12.011 Aº. This peak is related to the crystallographic plane and the zeolitic pore inside the sepiolite needles which cannot be modified by chemical modifications (Lima et al., 2017). Other characteristic peaks of sepiolite were 2θ= 19.7°, 20.6°, 23.7°, 26.4°, 27.9°, 35.0° and 36.7° are readily ascribed to (060), (131), (260), (080), (331) and (371) (Li et al., 2018). In the X-ray diffraction patterns of the gel-like dispersions, the main characteristic diffraction peaks of the sepiolite can be observed, interestingly, a new wider reflection between 15 and 23° and centering at ca. 19° is exhibited. This reflection is a typical amorphous one and it is assigned to the amorphous reflection of castor oil (Zhuang et al., 2018; Ford et al., 2010). As can be observed, the wide reflection of vegetable oil depends on sepiolite concentrations. When sepiolite content decreasing, the wide reflection of castor oil showed high intensity, indicating more oil molecules contained in the gel-like dispersion network.

The thermal degradation behaviors of the sepiolite, castor oil and selected gel-like dispersions with different clay contents (20, 30 and 40 wt.%) were investigated by the variation of percent mass loss with temperature (TGA curves) and differential mass loss with temperature (DTG curves). The TGA/DTG curves are presented in **Fig. 8**. Thermal decomposition of the castor oil takes place in one single stage between 300 and 495 ºC, attributable to the decomposition and/or volatilization of the ricinoleic fatty acid and subsequent degradation compounds. The thermal curve of sepiolite indicated that hydroscopic water from the external surface as well as zeolitic water from the voids of the structure were removed from 30 up to 130 °C with mass loss of 9%. Dehydration of the bound water found in magnesium coordination in the clay structure occurred in two steps; the first part of the bound water was lost between 130 and 305 °C with a percent

mass loss of 2.7% and the removal of bound water was completed at about 550 °C after a small plateau in the TGA curve and the percent mass loss became constant at 13% (Tanc and Orakdogen, 2019). Regarding thermal decomposition of gel-like dispersions, the weight loss rate curves (DTG), show two main thermal events, labelled as peaks P_1 and P_2. The first (P_1) peak located in the temperature range 210–290 ºC of the thermal degradation of gel-like dispersion may be associated to the dehydration of sepiolite, whereas the second (P_2) peak between 290 and 520 ºC would be related to the decomposition and/or volatilization of the castor oil (Gallego et al., 2015). Table 2 shows more relevant data obtained from the thermogravimetric analysis: the temperature for the onset of thermal decomposition (T_{onset}), the temperature at which decomposition rate is maximum (T_{max}) and the percentage of char yield (CY). As can be deduced from **Table 2**, the concentration of sepiolite has very small effect on the onset temperature (±2ºC) and maximum mass loss temperature of the gel-like dispersions.

3.3. Lubrication properties of gel-like dispersions

The effect of sepiolite content on some lubrication performance related properties of resulting gel-like dispersions has been analyzed according to some tribological experiments. **Table 3** shows consistency data of gel-like dispersions studied, as well as the corresponding NLGI grade. The NLGI grade is a commonly accepted parameter to classify lubricating greases as a function of their consistency degree (between 000 and 6) (NLGI, 1994). The most commonly used greases are those with NLGI grade 2. Softer grades, especially 0 and 1, are sometimes used for improved pumpability or low-temperature applications, while higher consistency indexes are used for certain high-speed bearings (Núñez et al., 2011). Obviously, NLGI grade increased with sepiolite content (between 0 and 4) and grade of sample prepared with 30 %wt. sepiolite was similar to the ones found in model bentonite lubricating grease (NLGI grade 2).

The suitability of these samples as lubricating greases was investigated in a tribological contact. **Fig. 9** shows the evolution of friction coefficient values with sepiolite content at different normal loads (10 N and 30 N) for gel-like dispersions studied as well as model bentonite grease. All samples showed a satisfactory response (values ranging from 0.088 to 0.155), the friction coefficient values increasing as sepiolite concentration became higher, and similarly, when lowering normal load. Interestingly, gel-like dispersions up to 30 wt.% showed lower friction coefficient values than model bentonite lubricating grease. These results demonstrate that the tribological behaviors of gel-like dispersions are affected by the sepiolite concentration. Gel-like dispersions with low linear viscoelastic functions have a greater capacity to form a protective lubricating film due to the rubbing action compared to gel-like dispersions with large linear viscoelastic functions, probably due to the interactions between sepiolite and molecular chain of the castor oil which hinder the motion of molecular chain of oil. Hence, it could be possible to optimize the sepiolite content in order to provide enough oil bleeding and at the same time the necessary consistency to produce a better replenishment at low-medium entrainment speeds, reducing friction.

In order to clearly explain the tribological behavior and wear mechanism, the morphologies of the wear scars generated in the plates of the tribological cell and the corresponding average diameter are shown in **Fig. 10** for selected gel-like dispersions and conditions. A rounded wear marks appear in all cases and the contact surfaces of steel balls are severely damaged. The worn surfaces show a rather rough trace and deep furrows along the sliding direction meaning that wear mechanism was predominantly abrasive. As can be observed, the wear degree and the contact area increase slightly when sepiolite content increases and the gel-like dispersions provided values of the average wear scar diameter higher to that found with model bentonite grease. Normal

load does not exert a significant influence (from 10N to 30N), nevertheless, when the stronger normal load is applied a slightly reduction the wear scar is, as can be seen in Fig. 10, which is in good accordance with the friction coefficient values previously obtained.

4. Conclusions

Gel-like dispersions based on sepiolite and castor oil were prepared to investigate the influence that sepiolite concentration exerts on the rheological, chemical, thermal properties and tribological performance in order to evaluate its applicability as thickening agent to develop eco-friendly lubricating greases. From the rheological point of view, samples showed important properties such as thixotropy, shear thinning and partial structure recovery. Linear viscoelastic functions of dispersions revealed a gel-like rheological behaviour, which was related to the development of sepiolite three-dimensional physical network due to the interaction among nanoscale fibers, laths and bundles of the sepiolite dispersed in the oil medium. The interweave of nanofibers (laths and bundles) of nanolayers enhanced the network structure, showing a gel strength that depended on sepiolite content. The mechanical rheo-reversibility (destruction and recovery) depended on the sepiolite concentration. The percentage of destruction decreased with the sepiolite content, while the percentage of recovery increased. All the samples exhibited shear-thinning behaviour over a wide range of shear rates, with the tendency to approach infinite-shear limiting viscosities, which fitted the Sisko model up to the concentration of 30 wt.%. Conversely, above this value gel-like dispersions showed fracture and expelling of sample. FTIR and XRD analysis of gel-like dispersions confirmed the presence of the main characteristic peaks of the sepiolite and also revealing that a new wider reflection assigned to the amorphous reflection of castor oil, which depended on sepiolite concentration. Thermal decomposition of gel-like

dispersions showed two peaks related to castor oil and sepiolite decomposition, with only a slight shift in their positions, which might be attributed to interaction between both components. Finally, all gel-like dispersions studied showed a satisfactory response, the friction coefficient values increased when sepiolite concentration became higher, and similarly, when lowering normal load. Interestingly, gel-like dispersions up to 30 wt.% showed lower friction coefficient values than model bentonite lubricating grease. The wear marks obtained after the frictional tests turned into slightly higher when sepiolite concentration increased and when a lower normal load was applied.

The present work follows as a continuation of recent research about the development of thickener agents to produce sustainable oleogels (Nuñez et al., 2012a; Martín-Alfonso, et al., 2011; Gallego, et al., 2015) for lubricant purposes, however, an new approach has been presented here using sepiolite clay as thickener. The results reported here allow the contribution from the sepiolite clay to the colloidal network observed in these gel-like dispersions to be computed. Notwithstanding, the promising rheological and tribological properties found at room temperature, and the valorization of this type of materials from an environmental and economic point of view to produce gel-like dispersions, the response at molecular level of these systems attending to friction tests and wear scar is not utterly clear. In short, oncoming works are needed to obtain more information about the tribological behaviour with the temperature or some mechanical tests usually employed to check lubrication performance and stability of lubricating greases in order to give some light on the real applicability of these formulations as lubricating greases.

References

Barnes, H.A., 1995. A review of the slip (wall depletion) of polymer solutions, emulsions and particle suspensions in viscometers: its cause, character, and cure. J. Non-Newtonian Fluid Mech. 56, 221–251.

1 Bergaya, F., Theng B.K.G., Lagaly, G., 2006. Handbook of clay science, First ed.
2 Elsevier, Amsterdam.

3 Castro-Smirnov, F.A., Piétrement, O., Aranda, P., Bertrand, J.R., Ayache, J., Cam, E.L.,
4 Ruiz-Hitzky, E., Lopez, B.S., 2016. Physical interactions between DNA and sepiolite
5 nanofibers, and potential application for DNA transfer into mammalian cells. Sci. Rep.
6 6, 36341.

7 Cavallaro, G., Chiappisi, L., Pasbakhsh, P., Gradzielski, M., Lazzara, G., 2018. A
8 structural comparison of halloysite nanotubes of different origin by Small-Angle
9 Neutron Scattering (SANS) and Electric Birefringence. Appl. Clay Sci. 160, 71–80.

10 Chtourou, M., Hédi Frikha, M., Trabelsi, M., 2006. Modified smectitic Tunisian clays
11 used in the formulation of high performance lubricating greases. Appl. Clay Sci. 32,
12 210–216.

13 Darder, M., Matos, C.R.S., Aranda, P., Gouveia, R.F., Ruiz-Hitzky, E., 2017.
14 Bionanocomposite foams based on the assembly of starch and alginate with sepiolite
15 fibrous clay. Carbohydr. Polym. 157, 1933–1939.
16 De Lima, J.A., Camilo, F.F., Faez, R., Cruz, S.A.A., 2017. A new approch to sepiolite
17 dispersion by treatment with ionic liquids. Appl. Clay Sci. 143, 234–240.

18 Du, P., Yuan, P., Thill, A., Annabi-Bergaya, F., Liu, D., Wang, S., 2017. Insights into
19 the formation mechanism of imogolite from a full-range observation of its sol-gel
20 growth. Appl. Clay Sci. 150, 115–124.

21 Fernandez-Barranco, C., Kozioł, A.E., Skrzypiec, K., Rawski, M., Drewniak, M.,
22 Yebra-Rodriguez, A., 2016. Reprint of study of spatial distribution of sepiolite in
23 sepiolite/polyamide6,6 nanocomposites. Appl. Clay Sci. 127–128, 129–133.

Ford, E.N.J., Mendon, S.K., Thames, S.F., Ph, D., Rawlins, J.W., Ph, D., 2010. X-ray diffraction of cotton treated with neutralized vegetable oil-based macromolecular crosslinkers. J. Eng. Fiber Fabr. 5, 10–20.

Galindo-Rosales, F.J., Rubio-Hernández F.J., 2006. Structural breakdown and build-up in bentonite dispersions. Appl. Clay Sci. 33, 109–115.

Gallego, R., Arteaga, J.F., Valencia, C., Franco, J.M., 2015. Thickening properties of several NCO-functionalized cellulose derivatives in castor oil. Chem. Eng. Sci. 134, 260–268.

Güngör, N., Işçi, S., Günister, E., Miśta, W., Teterycz, H., Klimkiewicz, R., 2006. Characterization of sepiolite as a support of silver catalyst in soot combustion. Appl. Clay Sci. 32, 291–296.

Lawal, O.S., Lapasin, R., Bellich, B., Olayiwola, T.O., Cesàro, A., Yoshimura, M., Nishinari, K., 2011. Rheology and functional properties of starches isolated from five improved rice varieties from West Africa. Food Hydrocolloids 25, 1785-1792.

Li, Y., Wang, M., Sun, D., Li, Y., Wu, T., 2018. Effective removal of emulsified oil from oily waste water using surfactant modified sepiolite. Appl. Clay Sci.157 227-236.

Liang, B., Li, R., Zhang, Ch., Yang, Z., Yuan, T., 2019a. Synthesis and characterization of a novel tri-functional bio-based methacrylate prepolymer from castor oil and its application in UV-curable coatings. Ind. Crops Prod. 135, 170–178.

Liang, D., Zhang, Q., Zhang, W., Liu, L., Liang, H., Quirino, R.L., Jie Chen, J., Liu, M., Lu, Q., Chaoqun Zhang, Ch., 2019. Tunable thermo-physical performance of castor oil-based polyurethanes with tailored release of coated fertilizers. J. Clean. Prod. 210, 1207-1215.

Magnin, A., Piau, J.M., 1990. Cone-and-plate rheometry of yield stress fluids. Study of an aqueous gel. J. Non-Newtonian Fluid Mech. 36, 85–108.

Maqueda, C., Partal, P., Villaverde, J., Perez-Rodriguez, J.L., 2009. Characterization of sepiolite-gel-based formulations for controlled release of pesticides, Appl. Clay Sci. 46, 289-295.

Martín Alfonso, J.E., Yañez, R., Valencia, C., Franco, J.M., Díaz, M.J., 2009. Optimization of the methylation conditions of kraft cellulose pulp for its use as a thickener agent in biodegradable lubricating greases, Ind. Eng. Chem. Res. 48, 6765-6771.

Martín Alfonso, J.E., Nuñez, N., Valencia, C., Franco, J.M., Díaz, M.J., 2011. Formulation of new biodegradable lubricating greases using ethylated cellulose pulp as thickener agent, J. Ind. Eng. Chem. 17, 818–823.

Martín-Alfonso, J.E., Romero, A., Valencia, C., Franco, J.M., 2013a. Formulation and processing of virgin and recycled polyolefin/oil blends for the development of lubricating greases. J. Ind. Eng. Chem. 19, 580-588.

Martín-Alfonso, J.E., Valencia, C., Sánchez, M.C., Franco, J.M., Gallego, C., 2013b. The effect of recycled polymer addition on the thermorheological behavior of modified lubricating greases. Polym. Eng. Sci. 53, 818–826.

Martín Alfonso, J.E., Franco, J.M., 2014. Ethylene-vinyl acetate copolymer (EVA)/sunflower vegetable oil polymer gels: Influence of vinyl acetate content. Polym. Test. 37, 78–85.

Martín Alfonso, J.E., Valencia, C., 2015. Tribological, rheological, and microstructural characterization of oleogels based on EVA copolymer and vegetables oils for lubricant applications. Tribol. Int. 90, 426–434.

Masood, F., Haider, H., Yasin, T., 2019. Sepiolite / poly-3-hydroxyoctanoate nanocomposites: Effect of clay content on physical and biodegradation properties. Appl. Clay Sci. 175, 130–138.

Mejía, A., García, N., Guzmán, J., Tiemblo, P., 2014. Surface modification of sepiolite nanofibers with PEG based compounds to prepare polymer electrolytes. Appl. Clay Sci. 95, 265–274.

NLGI, 1994. Lubricating Greases Guide. National Lubricating Greases Institute, Kansas City.

Núñez, K., Gallego, R., Pastor, J.M., Merino, J.C., 2014. The structure of sepiolite as support of metallocene co-catalyst during in situ polymerization of polyolefin (nano) composites. Appl. Clay Sci. 101, 73–81.

Nuñez, N., Martín-Alfonso, J.E., Eugenio, M.E., Valencia, C., Díaz, M.J., Franco, J.M., 2012a. Influence of eucalyptus globulus kraft pulping severity on the rheological properties of gel-like cellulose pulp dispersions in castor oil. Ind. Eng. Chem. Res. 51, 9777–9782.

Núñez, N., Martín-Alfonso, J.E., Valencia, C., Sánchez, M.C., Franco, J.M., 2012b. Rheology of new green lubricating grease formulations containing cellulose pulp and its methylated derivative as thickener agents. Ind. Crops Prod. 37, 500-507.

Olivato, J.B., Marini, J., Pollet, E., Yamashita, F., Grossmann, M.V.E., Avérous, L., 2015. Elaboration, morphology and properties of starch/polyester nano-biocomposites based on sepiolite clay. Carbohydr. Polym. 118, 250–256.

Özdemir, O., Çınar, M., Sabah, E., Arslan, F., Çelik, M.S., 2007. Adsorption of anionic surfactants onto sepiolite. J. Hazard. Mater. 147, 625–632.

Pasbakhsh, P., Churchman, G.J., Keeling, J.L., 2013. Characterisation of properties of various halloysites relevant to their use as nanotubes and microfibre fillers. Appl. Clay Sci. 74, 47-57.

Qiu, S., Li, Y., Li, G., Zhang, Z., Li, Y., Wu, T., 2019. Robust superhydrophobic sepiolite-coated polyurethane sponge for highly efficient and recyclable oil absorption. ACS Sustainable Chem. Eng. 7, 5560−5567.

Ray, S.S., Bousmina, M., 2005. Biodegradable polymers and their layered silicate nanocomposites: in green the 21st century materials word. Prog Mater. Sci. 50, 962-1079.

Ruiz-Hitzky, E., Aranda, P., Alvarez, A., Santarén, J., Esteban-Cubillo, A., 2011. Advanced materials and new applications of sepiolite and palygorskite. In: Galan, E., Singer, A. (Eds.), Developments in Palygorskite–Sepiolite Research. A New Outlook of These NanomaterialsDevelopments in Clay Science 3. Elsevier, Amsterdam, pp. 393–452.

Ruiz-Hitzky, E., Darder, M., Fernandes, F.M., Wicklein, B., Alcântara, A.C.S., Aranda, P., 2013. Fibrous clays based bionanocomposites. Prog. Polym. Sci. 38, 1392–1414.

Rytwo, G., Tropp, D., Serban, C., 2002. Adsorption of diquat, paraquat and methyl green on sepiolite: experimental results and model calculations. Appl. Clay Sci. 20, 273–282.

Rytwo, G., Rettig, A., Gonen, Y., 2011. Organo-sepiolite particles for efficient pretreatment of organic wastewater: application to winery effluents. Appl. Clay Sci. 51, 390–394.

Sabah, E., 2007. Decolorization of vegetable oils: Chlorophyll-a adsorption by acid-activated sepiolite. J. Colloid Interface Sci. 310, 1-7.

Tanc, B., Orakdogen, N., 2019. Insight into (alkyl)methacrylate-based copolymer/sepiolite nanocomposite cryogels containing amino and sulfonic acid groups: Optimization of network properties and elasticity via cryogelation process. React. Funct. Polym. 140, 31–47.

Weng, J., Gong, Z., Liao, L., Lv, G., Tan, J., 2018. Comparison of organo-sepiolite modified by different surfactants and their rheological behavior in oil-based drilling fluids. Appl. Clay Sci. 159, 94–101.

Yeong, S.K., Luckham, P.F., Tadros, Th.F., 2004. Steady flow and viscoelastic properties of lubricating grease containing various thickener concentrations. J. Colloid Interface Sci. 274, 285–293.

Zhuang, G., Zhang, Z., Peng, S., Gao, J., Jaber, M., 2018. Enhancing the rheological properties and thermal stability of oil-based drilling fluids by synergetic use of organo-montmorillonite and organosepiolite. Appl. Clay Sci. 161, 505–512.

Figure Captions

Fig. 1. Dependence of the normalized storage modulus with stress (τ) for gel-like dispersions as function of sepiolite content.

Fig. 2. Frequency dependence of the storage and loss moduli (a) and tan δ (b), in the linear viscoelasticity region, for gel-like dispersions containing different sepiolite concentrations and model bentonite grease (filled symbols, G'; empty symbols, G'').

Fig. 3. Evolution of SAOS parameters (G'_1, G''_1 and tan δ_1) at 1 rad/s of gel-like dispersions studied, as a function of sepiolite concentration.

Fig. 4. a) Viscous flow curves of gel-like dispersions as function of sepiolite content and b) thixotropic and shear thinning properties of gel-like dispersions measured by plotting viscosity over time and at changing shear rates of 0.1 s^{-1} and 10 s^{-1}.

Fig. 5. Complex modulus (G*) decay, at frequency of 1 Hz, after changing shear strain from the linear to the nonlinear viscoelastic region and further recovery when the former shear strain is reimposed for the evolution of complex modulus for gel-like dispersions containing different sepiolite concentrations.

Fig. 6. (a) FTIR spectra of the sepiolite and castor oil; (b) FTIR spectra for selected gel-like dispersions as a function of sepiolite concentration.

Fig. 7. X-Ray diffractograms for gel-like dispersions as a function of sepiolite concentration. Pure sepiolite intensity profiles are also included for reference.

Fig. 8. TGA thermograms for pure sepiolite, castor oil and selected gel-like dispersions as a function of sepiolite concentration.

Fig. 9. Stationary friction coefficient values at different normal loads (10 and 30N) as a function of sepiolite concentration for gel-like dispersions studied.

Fig. 10. Optical images and corresponding average diameter of the worn plate surface for steel/steel contacts obtained at 25 °C, constant rotational speed (100 rpm) and different normal loads (10 and 30N) using selected gel-like dispersions: A, B) 20 wt.% Sep; C, D) 30 wt.% Sep; E, F) 40 wt.% Sep; G, H) model bentonite grease.

.

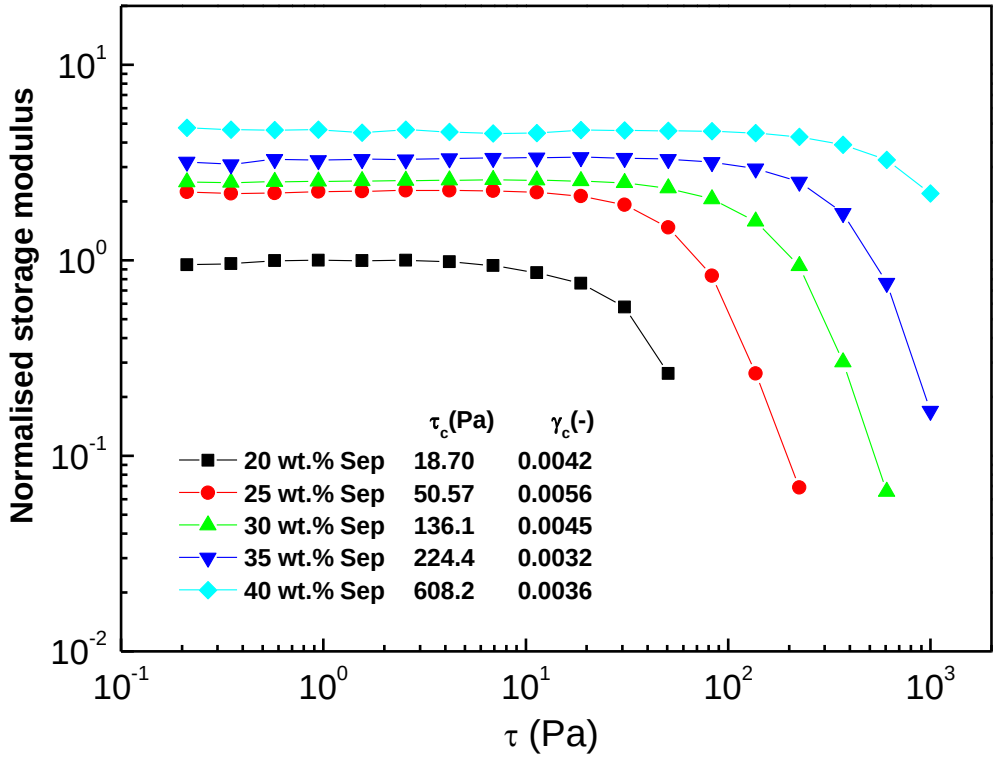
Normalised storage modulus
τ (Pa)
τc(Pa)
γc(-)
20 wt.% Sep 18.70 0.0042
25 wt.% Sep 50.57 0.0056
30 wt.% Sep 136.1 0.0045
35 wt.% Sep 224.4 0.0032
40 wt.% Sep 608.2 0.0036

Fig. 1.

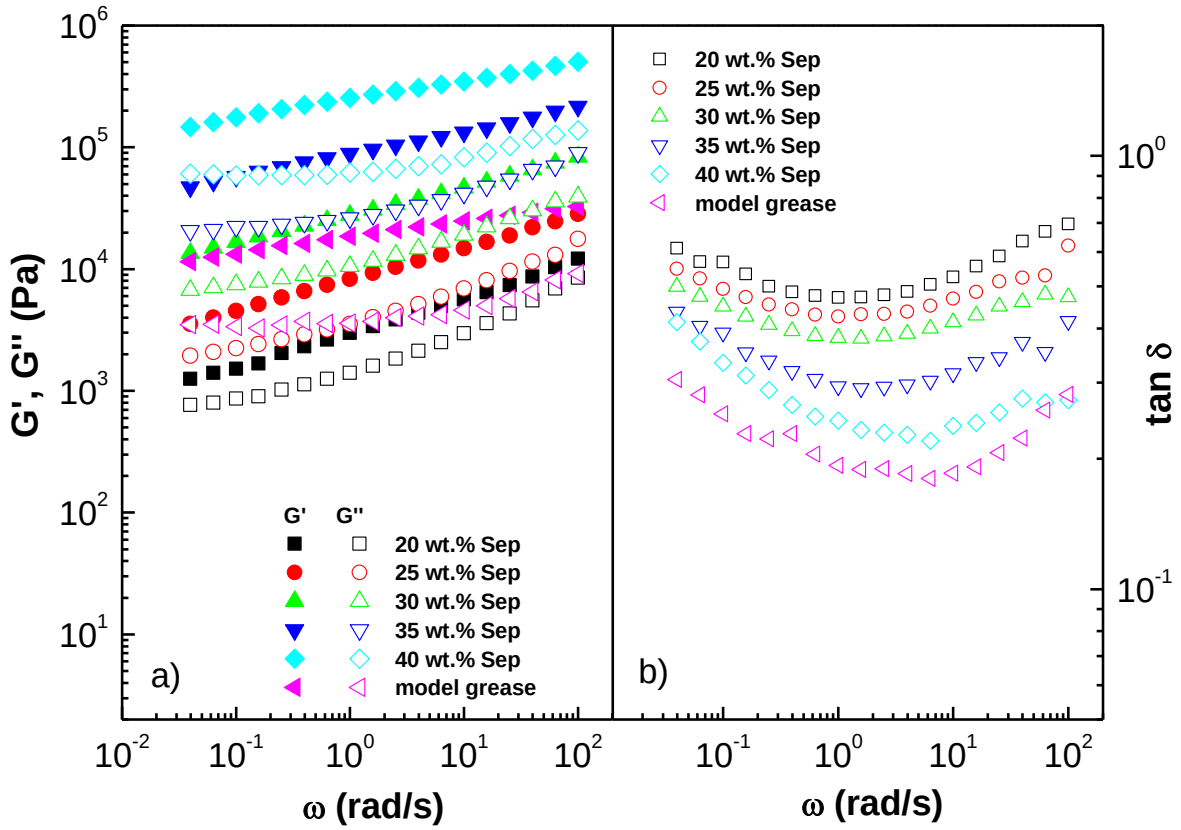
G', G'' (Pa)
ω (rad/s)
tan δ
a)
b)
G'
G''
20 wt.% Sep
25 wt.% Sep
30 wt.% Sep
35 wt.% Sep
40 wt.% Sep
model grease

Fig. 2.

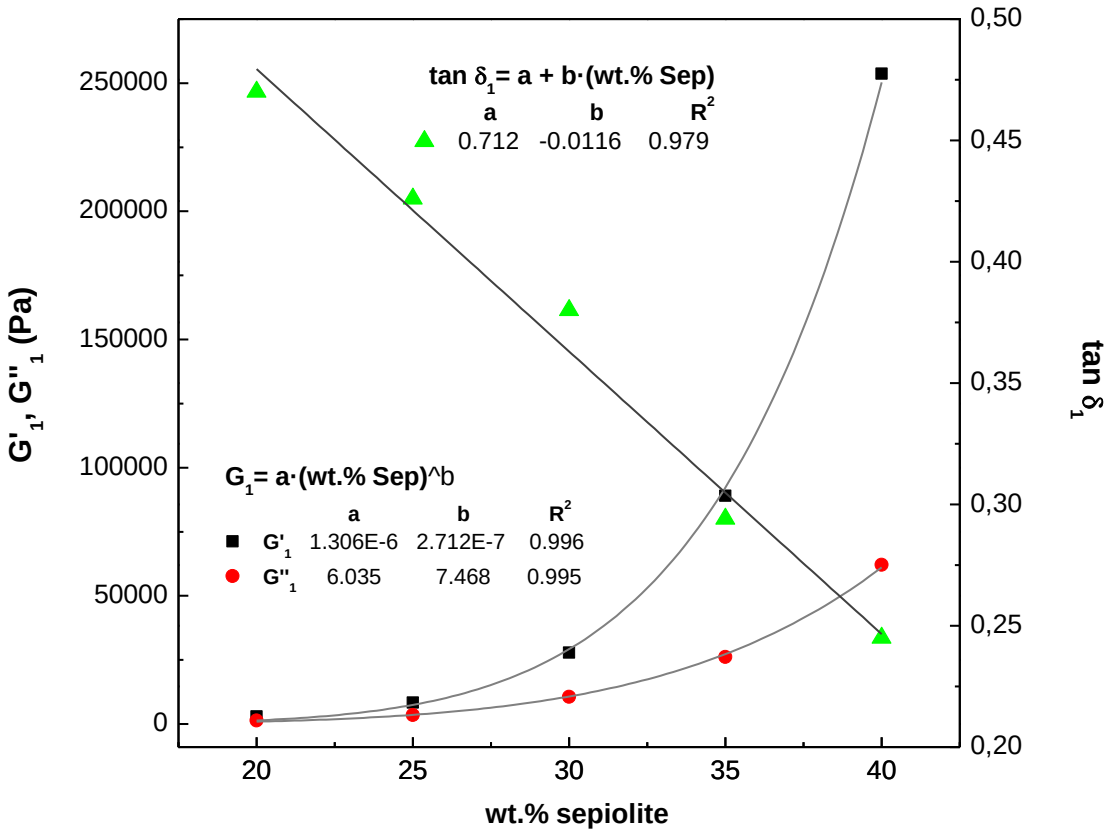
tan δ1= a + b·(wt.% Sep)
a b R2
0.712 -0.0116 0.979
G1= a·(wt.% Sep)^b
a b R2
G'1 1.306E-6 2.712E-7 0.996
G''1 6.035 7.468 0.995
G'1, G''1 (Pa)
tan δ1
wt.% sepiolite
250000
200000
150000
100000
50000
0
0,50
0,45
0,40
0,35
0,30
0,25
0,20
20
25
30
35
40

Fig. 3.

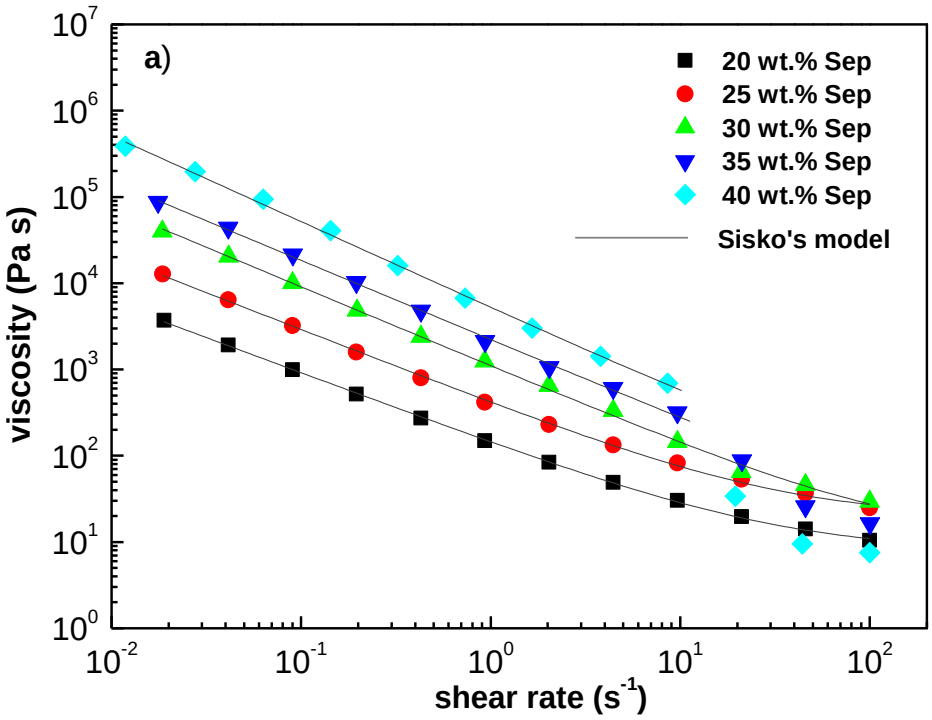
a)
20 wt.% Sep
25 wt.% Sep
30 wt.% Sep
35 wt.% Sep
40 wt.% Sep
Sisko's model
viscosity (Pa s)
shear rate (s-1)

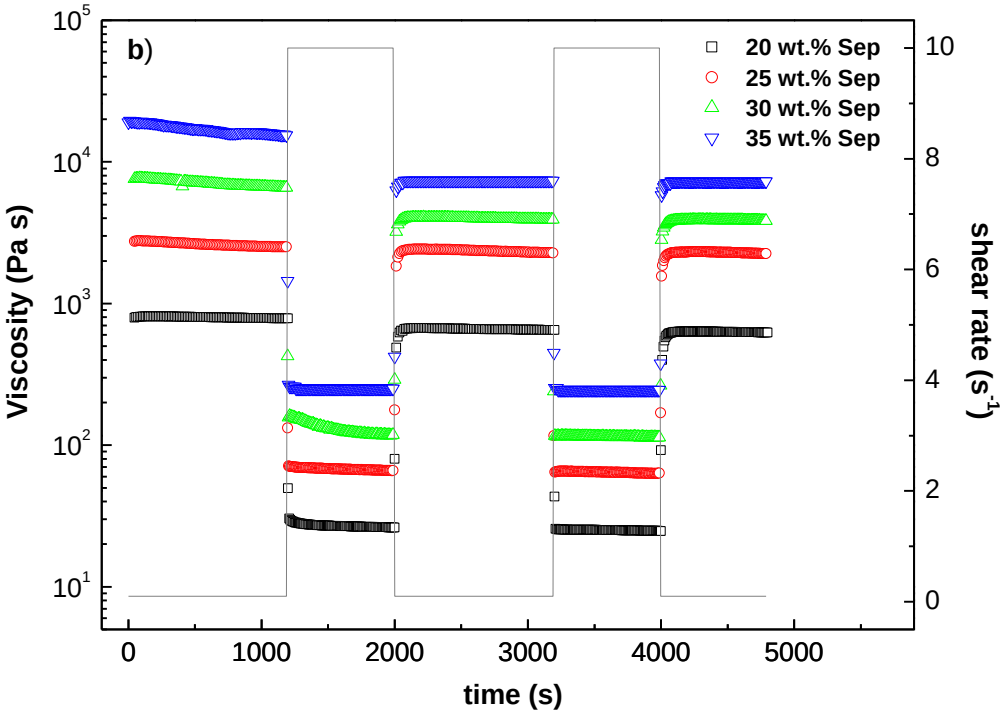
b)
20 wt.% Sep
25 wt.% Sep
30 wt.% Sep
35 wt.% Sep
Viscosity (Pa s)
shear rate (s-1)
time (s)

Fig. 4.

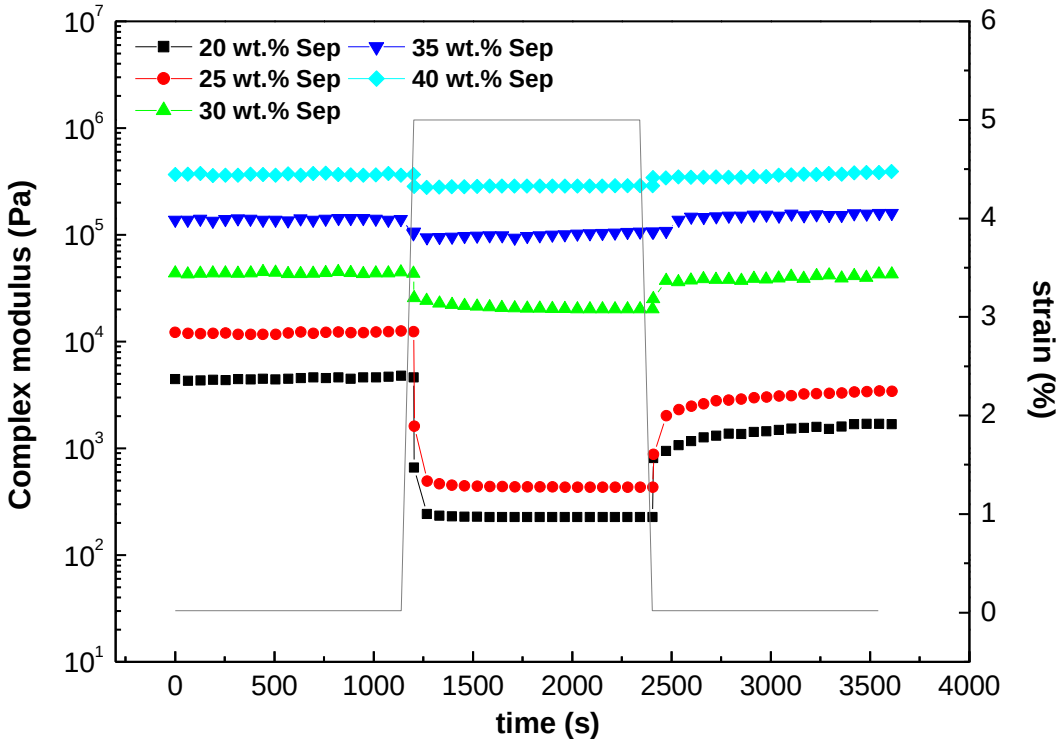
20 wt.% Sep
25 wt.% Sep
30 wt.% Sep
35 wt.% Sep
40 wt.% Sep
Complex modulus (Pa)
strain (%)
time (s)
10^7
10^6
10^5
10^4
10^3
10^2
10^1
6
5
4
3
2
1
0
0
500
1000
1500
2000
2500
3000
3500
4000

Fig. 5.

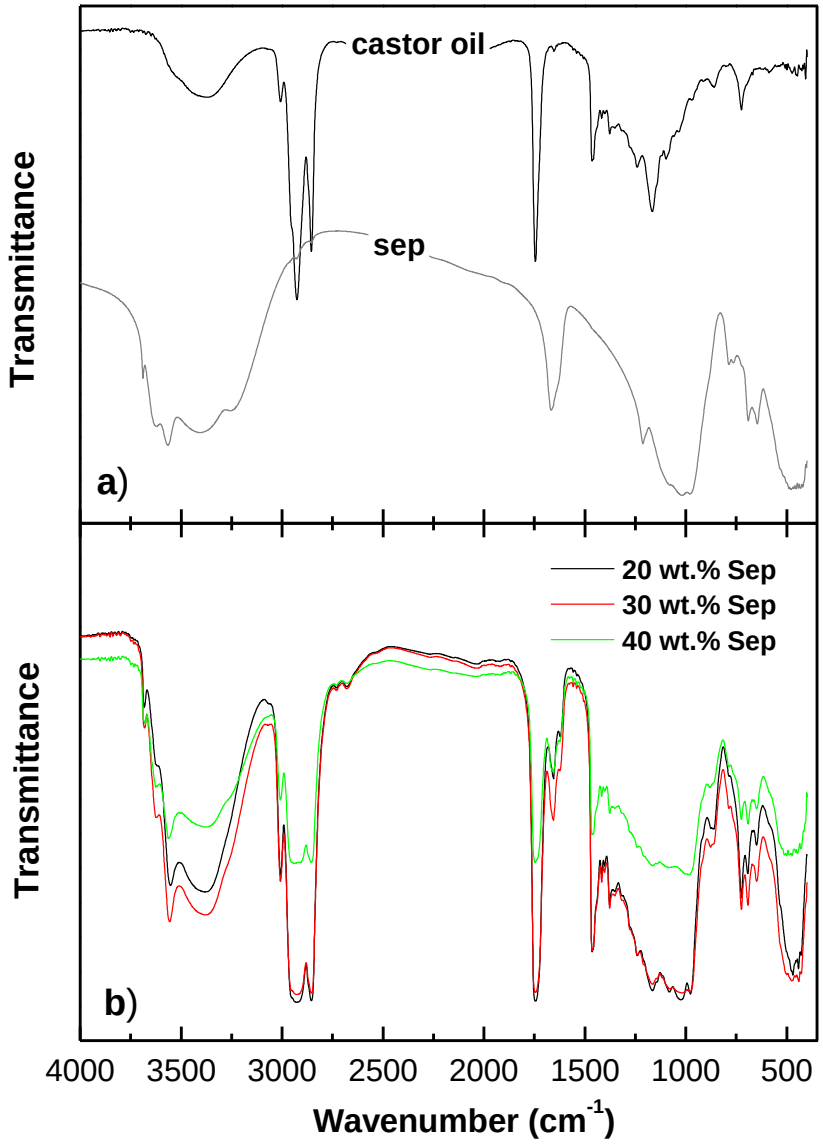
castor oil
sep
Transmittance
a)
20 wt.% Sep
30 wt.% Sep
40 wt.% Sep
Transmittance
b)
4000
3500
3000
2500
2000
1500
1000
500
Wavenumber (cm-1)

Fig. 6.

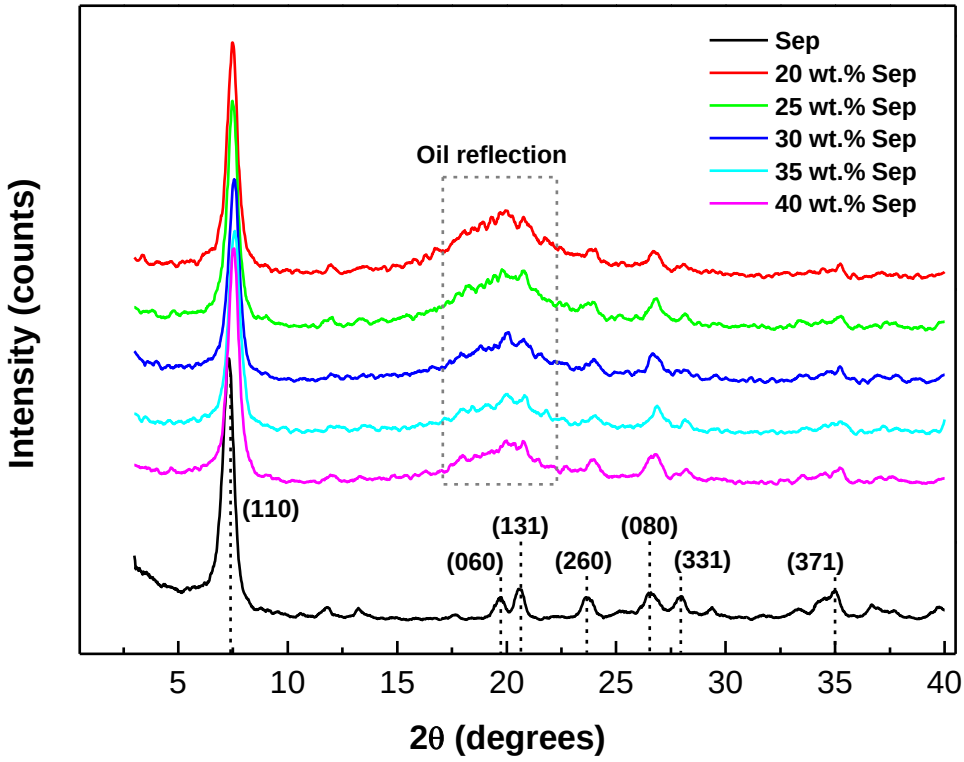
Sep
20 wt.% Sep
25 wt.% Sep
30 wt.% Sep
35 wt.% Sep
40 wt.% Sep
Oil reflection
(110)
(060)
(131)
(260)
(080)
(331)
(371)
Intensity (counts)
2θ (degrees)
5
10
15
20
25
30
35
40

Fig. 7.

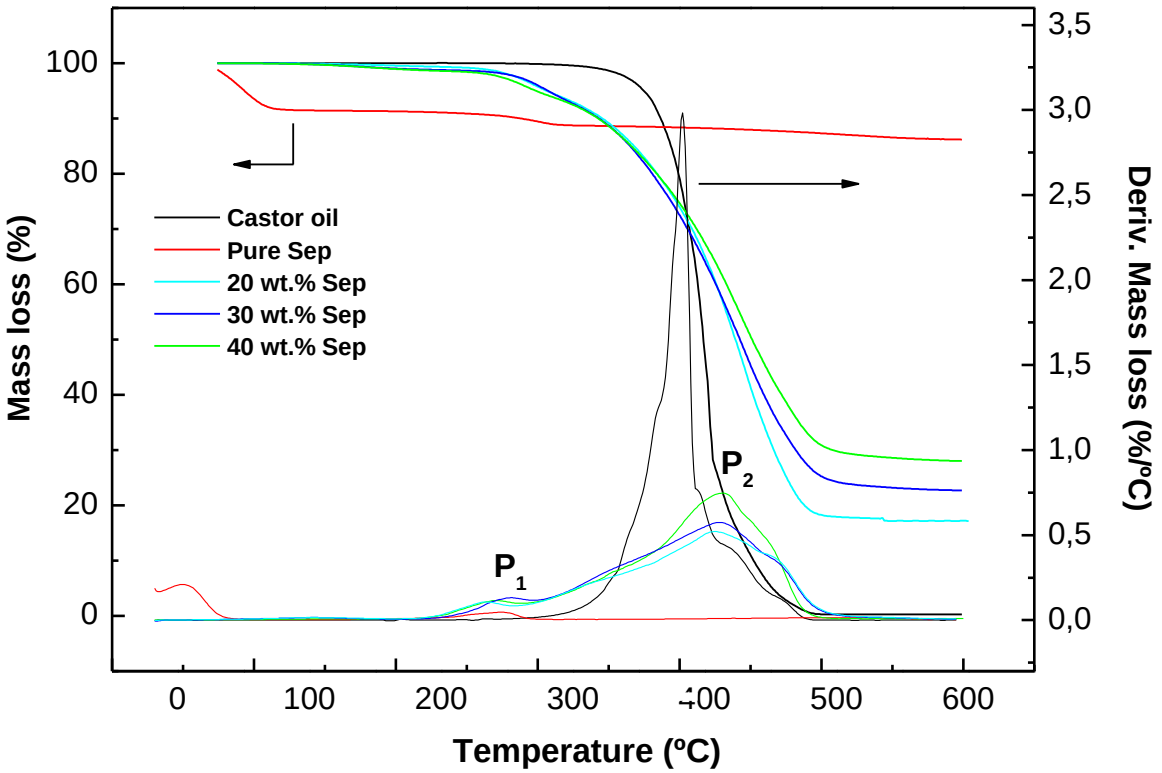
Mass loss (%)
Deriv. Mass loss (%/°C)
Temperature (°C)
Castor oil
Pure Sep
20 wt.% Sep
30 wt.% Sep
40 wt.% Sep
P1
P2
0
20
40
60
80
100
0,0
0,5
1,0
1,5
2,0
2,5
3,0
3,5
0
100
200
300
400
500
600

Fig. 8.

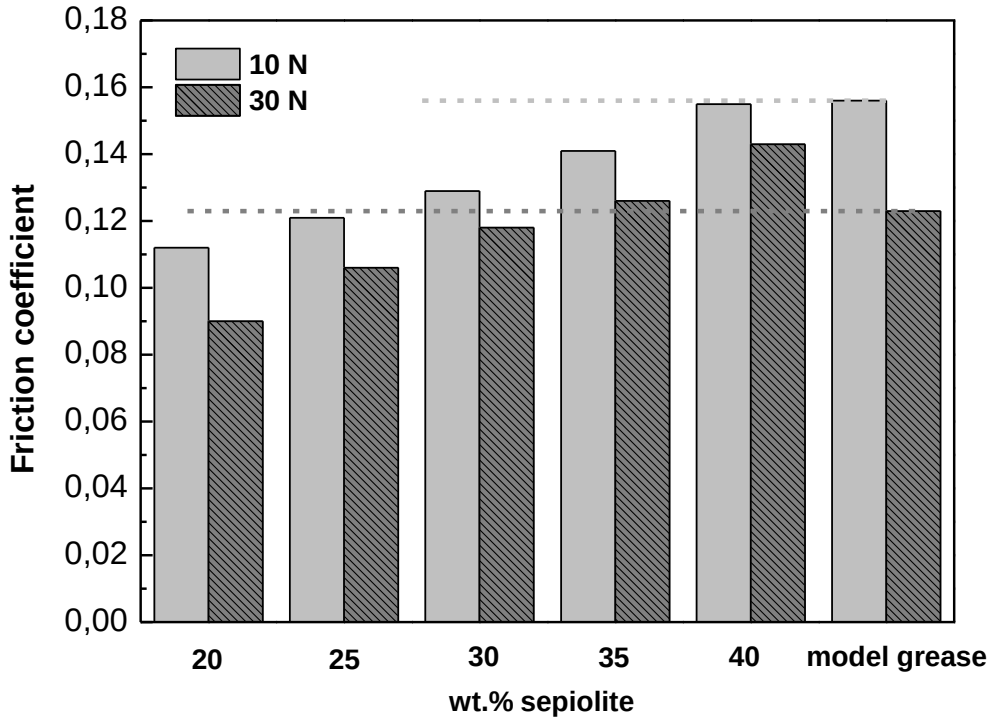
0,18
0,16
0,14
0,12
0,10
0,08
0,06
0,04
0,02
0,00
Friction coefficient
10 N
30 N
20
25
30
35
40
model grease
wt.% sepiolite

Fig. 9.

10N	30N
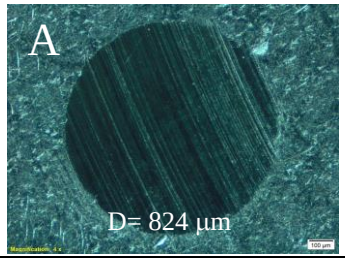	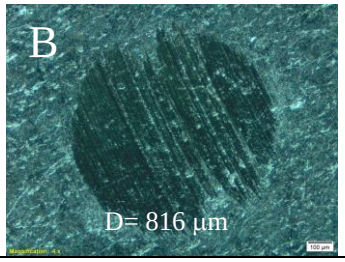
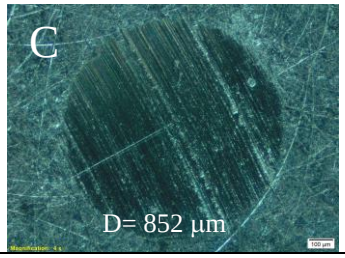	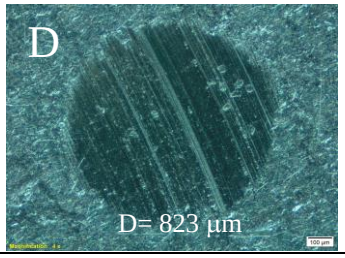
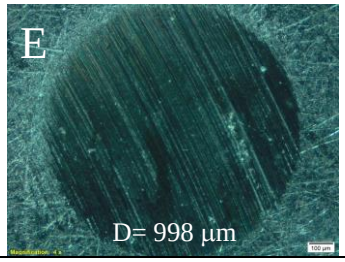	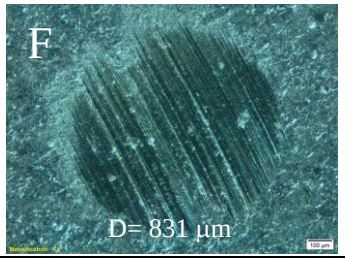
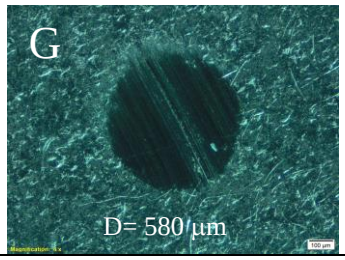	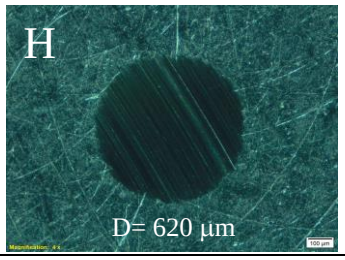

Fig. 10.

Table 1. Rheological parameters for gel-like dispersions studied.

Samples	m (Pa·s^n)	n	η_∞ (Pa s)	Destruction (%)	Recovery (%)
20 wt.% Sep	137.5	0.179	7.785	94.89	31.58
25 wt.% Sep	401.1	0.142	19.45	96.28	24.71
30 wt.% Sep	1095.4	0.082	11.71	54.11	77.67
35 wt.% Sep	2212.8	0.080	-	28.73	97.34
40 wt.% Sep	5216.1	0.030	-	21.28	98.46
model grease	810.3	0.014	3.082	75.27	49.32

Table 2. Thermal property data for gel-like dispersions (subscripts 1–2 refer to P_1–P_3 peaks in Fig. 8, respectively).

Samples	T_{onset} (°C)[a]	T_{max1} (°C)[b]	T_{max2} (°C)[b]	CY (%)[c]
20 wt.% Sep	280.2	271.4	430.6	17.7
25 wt.% Sep	281.1	282.1	422.3	21.1
30 wt.% Sep	280.6	281.3	428.7	22.8
35 wt.% Sep	281.3	273.7	425.3	24.8
40 wt.% Sep	279.8	263.5	424.5	28.1

[a] Temperature at 5 mass % loss.

[b] Maximum mass loss temperature.

[c] CY: char yield, the residue after TGA analysis at a maximum temperature of 600 °C.

Table 3. NLGI consistency numbers and penetration values for gel-like dispersions studied.

Samples	penetration index (dmm)	NLGI grade
20 wt.% Sep	500	000
25 wt.% Sep	430	00
30 wt.% Sep	301	1-2
35 wt.% Sep	252	3
40 wt.% Sep	219	3-4
model grease	280	2